ORIGINAL ARTICLE

Experimental investigations on early crack development in fully restrained reinforced concrete members with active zero-displacement control

Christopher Schmidt (ORCID) **· Rostislav Chudoba · Chao Jin · Josef Hegger**

Abstract The development of restraint-induced stress in reinforced concrete members at an early age can be tested using setups applying either passive or active displacement control. To provide results relevant for the practical design of minimum reinforcement to limit the crack width, an actively controlled test setup for large specimens was developed to perform a systematic experimental campaign focusing on the early crack development under well-defined mechanical and thermal boundary conditions. The full degree of restraint achieved by actively preventing any displacement of the member allowed for the theoretical interpretation of early restraint-induced stress evolution, deformation behaviour in the cracked and uncracked regions, and reinforcement stress for a variety of parameters, including hydration rates, member height, bar diameters and subsequently reinforcement ratio. The cracking process, starting with primary cracks accompanied by secondary cracks within the effective reinforcement area, is monitored in combination with the development of the tensile strength and Young's modulus of the concrete. Furthermore, the time of cracking and the forces released upon crack occurrence, considering the effect of self-equilibrating stresses, are determined, analysed, and compared with the results of crack-force based design rules to determine the minimum amount of reinforcement that ensures the crack width limitation.

1 Introduction

In most structural systems, voluminous concrete members such as walls, slabs and shells are exposed to restrained displacement boundary conditions. This results in tensile stress occurring due to the partial or full prevention of free deformation, which can lead to cracking. To limit the crack width, the amount of reinforcement must be determined in such a way that a sufficiently small crack spacing and crack width are ensured. The design of this reinforcement amount is of special interest for thick members [1–4], high degrees of restraint [5, 6], and design situations with special requirements for crack width control [7].

In early concrete age, the hydration induced temperature development in a restrained structure leads to induced strains. The resulting restraint-induced stress is influenced by the concrete's Young's modulus development and early creep behaviour

C. Schmidt (✉) · R. Chudoba · C. Jin · J. Hegger
Institute of Structural Concrete, RWTH Aachen
University, Mies-van-der-Rohe-Straße 1, 52074 Aachen,
Germany
e-mail: cschmidt@imb.rwth-aachen.de

[8–10]. Following the temperature rise in the first phase of the concrete hydration, the subsequent cooling down phase of the member increases the tensile stress that can reach the concrete tensile strength, leading to early crack occurrence [11, 12]. Beyond the early age, sustained long-term stress development can lead to tension as high as the tensile strength, causing late cracking [13, 14].

Shrinkage induces strains which are part of the overall restraint-induced stress under restrained condition. During concrete hydration, chemical and autogenous shrinkage occur, with strain values decreasing at the end of the hydration process. The moisture transport between the concrete member and the environment leads to drying shrinkage. The resulting moisture variations in the specimen depend on the geometrical properties and the thermal boundary conditions. For example, upon the removal of the formwork a high moisture flux between the member and the ambient air occurs, resulting in increasing shrinkage strains. Such a change of the moisture content in the concrete member affects the magnitude of drying shrinkage strain. The interaction of shrinkage with the hydration-related temperature development during the early age of concrete [15, 16] or with e.g. high magnitudes of ambient temperature [17] over the service life [18, 19] induces tension in a restrained member that provokes cracking.

For restraint-induced stress the free deformation must be prevented. The degree of which this free deformation is restrained influences the magnitude of the stress, an increasing degree of restraint significantly increases the restraint-induced stress and therefore influences the time of first cracking and the number of cracks [20–24]. When conducting experimental investigations on restraint members, the degree of restraint must be accounted for in the test setup. A good overview of different test setups to conduct restraint tests on concrete specimens with and without reinforcement can be found in [25, 26]. Commonly used are passive frames placed around the reinforced concrete specimens to restrain their displacement [27] or plain concrete rings [28]. The degree of restraint depends on the frame stiffness. To investigate the cracking behaviour, especially for large specimens, a frame with a very high stiffness is necessary to simulate the high forces that occur in the configuration of an infinite slab. An example is provided by the CEOS.fr project [24], where reinforced concrete slabs

with a cross-section of up to 0.4 m² were tested under exterior conditions with a passive frame consisting of steel bars and solid concrete blocks at the specimen ends.

As an alternative to partially restrained systems, an actively controlled test setup that ensures zero change in the specimen length can be used to introduce a fully restrained state, often referred to in the literature as 'Temperature Stress Testing Machine'. The actively controlled displacement is either achieved by an applied displacement counteracting the occurred deformation of the specimen [29, 30] or is equivalent to the free deformation of a specimen without restrained deformation tested under identical thermal conditions [20, 31–33]. In addition to tests with unreinforced specimens [20, 29, 31, 32], multiple-cracking behaviour of restrained steel-reinforced concrete members has been investigated in [30, 33]. The type of displacement control, either continuous or stepwise and its timing, has a significant influence on the development of the restraint-induced stress. Moreover, to ensure reproducible results, test series with controlled, constant climate conditions were introduced, using either insulated formwork, e.g. in [27, 29], or climate-controlled rooms, e.g. in [20]. Due to practical limitations in the laboratory, these series were often limited to smaller specimen sizes.

To gain a deeper insight into the stress development and cracking behaviour of restrained members in early concrete, an experimental program was conducted testing reinforced concrete slabs under partially and fully restrained conditions. The restraint-induced stress is caused by the temperature development due to hydration and shrinkage without additional external stress loading. To provoke early cracking under defined restrained boundary conditions during the test, a setup with active displacement-controlled loading has been developed. It prevents the global elongation of the specimens under steady ambient climate conditions, which is controlled by an integrated air conditioning system. Systematic variation of the test parameters, namely the member height, hydration rate of the concrete mixture, reinforcement ratio and bar diameter, has been used to study their effect on the restraint-induced stress development, cracking, and post-cracking behaviour. The results are discussed in view of the design-relevant characteristics such as tensile strength at the time of crack occurrence, self-equilibrating stress profile, steel

stress development and bond strength. In design codes such as *fib* Model Code 2010 or Eurocode 2, the mentioned characteristics are used to determine the minimal amount of reinforcement required to ensure the crack width limit and consequently the durability of the structural member.

2 Restrained stress and crack development at early age

The temperature field in a structural member is conditioned by the concrete mixture, the cross-sectional geometry and the thermal boundary conditions [10, 20, 34, 35]. Any change in temperature leads to an increase in strain, which results in stress development under restrained deformation. Young concrete undergoes a large creep and relaxation process reducing the stress increase over time [36–38]. This viscoelastic material behaviour leads to a considerable and non-negligible reduction of the theoretical pure elastic stress evolution [20–22].

In the initial phase of the hydration process, the rising temperature induces compression under restrained condition. However, the maximum compression of the specimen occurs before the maximum concrete temperature is reached, as smaller strain increments add to the overall viscoelastically reduced stress field. The following cooling phase leads to stress reduction towards zero value, defined as the time of second zero-stress t_2. Because the stress field in a member is inhomogeneous, there is a certain time period in which all material points pass through the second zero-stress level. The progressive cooling and thus the growth of tensile strains increases the restraint-induced tensile stress, increasing faster over time due to the increase of the developing Young's modulus as well as to the different creep and relaxation behaviour of concrete under compression and tension [39–42]. When cracks occur, the restrained deformation is partially compensated by the crack opening, which depends on the fracture mechanics of concrete (e.g. calculation approaches in [43]) and the bond behaviour with the reinforcement. Further growth of strains and restraint-induced stresses leads to ongoing crack occurrence.

The crack formation process depends on the member height and reinforcement layout. While thin members typically exhibit only primary cracks running through the entire cross-section, secondary cracks occur in the boundary zone around the reinforcement in thick members [3, 7]. The crack tips of branched secondary cracks are typically directed towards the nearest primary crack. It is shown that the size of the boundary zone with secondary cracks increases with the member thickness [3]. In design codes such as the Eurocode 2 [44, 45], this dependency is taken into account by a linear relationship [7].

Restrained members exhibit a non-linear stress profile over height, consisting of a constant stress component induced by the global temperature change, a linear component due to different temperatures at the opposite surfaces, and a non-linear component caused by self-equilibrating stresses. The linear component of the stress profile becomes significant for dominating flexural restraint.

In general, cracking occurs when the decisive local tensile stress in the member reaches the concrete tensile strength $f_{ct,eff}$. Many design codes, e.g. [44, 46], assume a direct link between the crack-released force F_{cr} and the required minimum reinforcement A_s. Equation (1), adapted from [7, 45], displays this approach

$$F_{cr} = \sigma_{sr} \cdot A_s = f_{ct,eff} \cdot A_{c,eff.} \tag{1}$$

For this crack-force based approach, the tensile strength at the time of cracking and the effective concrete area under tension $A_{c,eff}$ must be known or assumed. In addition, the effect of self-equilibrating stress should be considered. Regarding the steel stress σ_{sr} in the crack, a kinematically based consideration of the strain difference between the reinforcement and concrete in the cracked area can estimate the maximum acceptable value of the steel stress to limit the crack width w_k. Simplifications consider a mean strain level for the reinforcement and the concrete. Neglecting the influence of shrinkage, it is assumed that the crack width equals twice the transfer length multiplied by the mean strain difference for a single crack running through the entire cross-section. The steel stress is then given by

$$\sigma_{sr} = \sqrt{\frac{2 \cdot w_k \cdot \tau_{bm} \cdot E_s \cdot (1 + \rho \cdot \alpha_e)}{d_s \cdot (1 - \beta)}}, \tag{2}$$

with the modular ratio $\alpha_e = E_s/E_c$, the reinforcement ratio $\rho = A_s/A_c$, and the bar diameter d_s. The design bond strength τ_{bm} is assumed to be constant over the transfer length and is usually approximated as a

function of the concrete tensile strength. The influence of a bond-free length at the crack itself is considered by a simplification, assuming a design bond strength $\tau_{bm} = 1.8f_{ct,eff}$, as proposed in design codes [45, 46]. To account for the actual non-linear bond behaviour over the length, a reduction factor β is used, which also considers additional effects such as bond creep under long-term loading [46, 47].

This crack-force based approach focuses only on the local discontinuity area around a single crack and neglects the behaviour of the whole member. Nevertheless, cracking in other areas affects the restrained deformation and the overall member stiffness as reported in [27, 48], by interacting with the stress development, the time-dependent material behaviour, the crack mechanism and the system's degree of restraint. Various approaches have been considered in the literature to account for the interaction between the local discontinuity region and the behaviour of the whole structural member. For example, the deformation compatibility reported in [48, 49] accounts for the actual restrained deformation of a member being equal to the deformation occurring in the uncracked concrete plus the total crack width. The existing criteria for thermally induced cracking [25] are distinguished into stress-based, strain-based, and combined and account for the time-dependent behaviour as well as the degree of restraint. However, the effect of the reinforcement and the member behaviour after the occurrence of the initial crack is not considered.

The influence of the named factors on the stress development and cracking behaviour of restrained reinforced concrete members at early age of concrete, the material variations, and the interactions of the factors with each other lead to a complex behaviour of the member. Therefore, the experimental campaign aims to isolate the effect of each factor on the structural response under well defined, and reproducible mechanical and thermal boundary conditions.

3 Experimental campaign

3.1 Test setup simulating a section in an infinite slab

The test setup used for the herein presented investigations is conceptualised aiming to represent a section of an infinite slab under centric tension due to

deformation restraint and concrete hydration. Therefore, the thermal and mechanical boundary conditions of this section are chosen to represent a large, restrained concrete slab in situ (Fig. 1). To simulate this condition, the surfaces representing the transitions to the surrounding infinite slab, corresponding to the x–z planes in Fig. 1, have been insulated throughout the testing phase to prevent almost all thermal flux. It is further assumed that no heat flux is possible in the regions of load introduction, being the y–z planes. On the following day after casting the specimen, the formwork of the surfaces in contact with the ambient air corresponding to the x–y planes marked in green was removed. The surfaces were enclosed in a climate-controlled containment ensuring constant ambient temperature and humidity, with a fixed ambient temperature of 17 °C and a relative humidity of 50%. This led to reproducible heat and moisture flux between the specimen and surrounding environment under steady ambient conditions, which were nearly equal for all specimens. The result of equal ambient temperatures on these surfaces is pure centric restraint. The full degree of restraint was achieved by preventing any movement of the specimen ends in the longitudinal (x-) direction with the active zero displacement control.

3.2 Active zero displacement control

In the present study, the test setup with actively controlled full restraint and ambient conditions was designed to allow for a rigorous theoretical interpretation of the experimental results. The full restraint represents the asymptotic case for the evolution of the maximum concrete compressive and tensile stresses that can occur in an infinite slab. In this configuration, the time of initial crack occurrence and the amount of stress released are not biased by any undefined free displacement of the specimen ends. In this form, the test results provide a sound basis for in-depth interpretations using theoretical and numerical models of early crack development. Examples of the use of test results as a basis for modelling the restraint-induced stress and early crack development can be found in [21, 50–52].

To achieve this fully restrained condition for large specimens, able to represent a section of an infinite slab, the test setup displayed in Fig. 2 has been developed. It employs a cylinder with the required
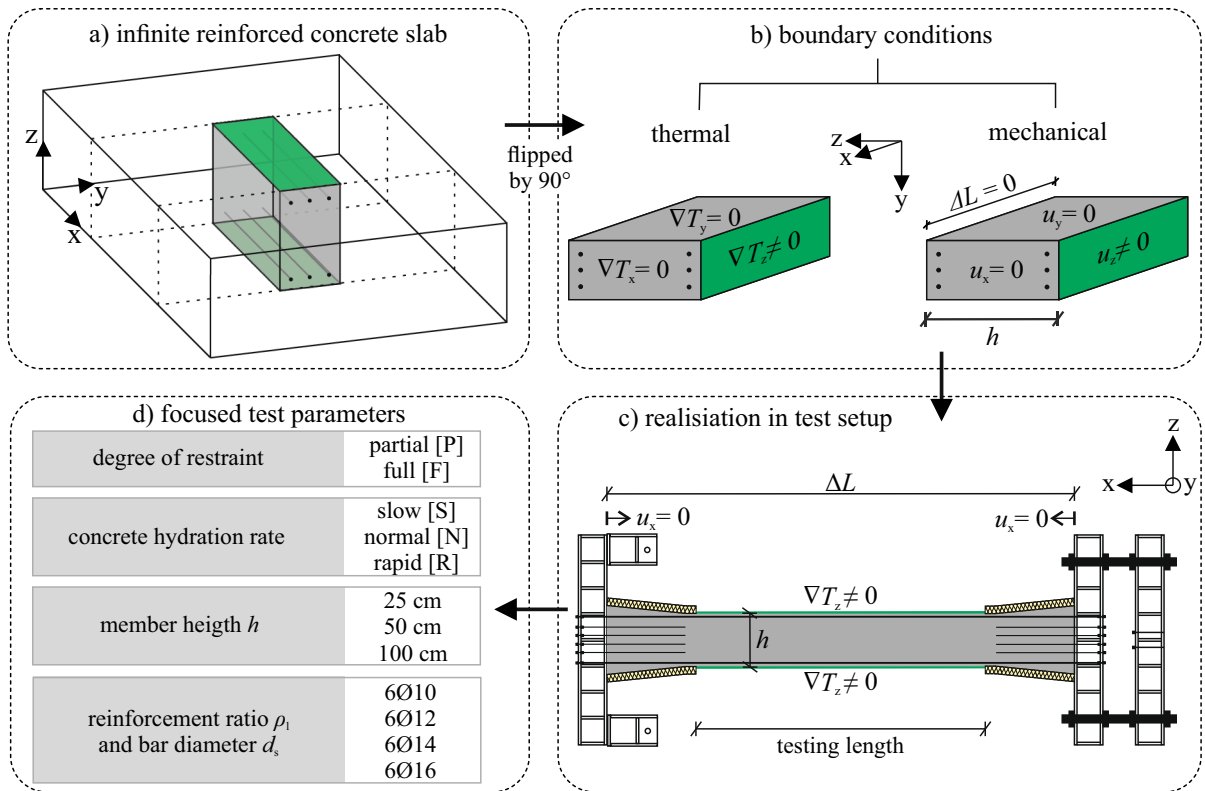
Fig. 1 Transferring the boundary conditions from an infinite slab towards a sectional representation in the test setup, with the investigated parameters
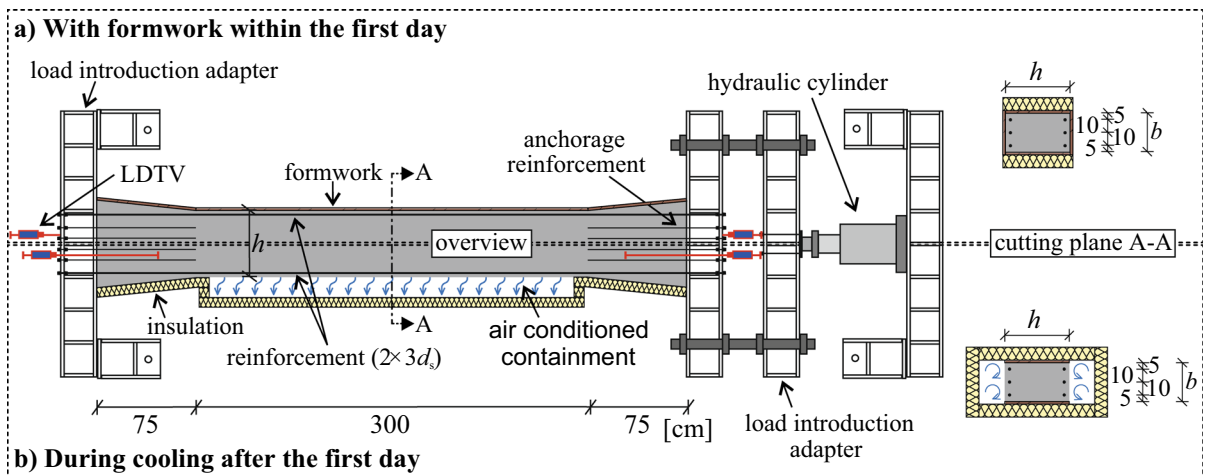

Fig. 2 Test setup with active zero displacement control for the two different phases of framing and air conditioning

load capacity of 1 MN, an air-conditioned containment to control the ambient temperature, and a sensor-based active load control system.

The cross-section in the load introduction area of each specimen was widened. Sufficient anchorage was ensured by additional reinforcement in this area (Fig. 2). The temperature sensors were attached to

vertical bars (z-direction) and placed at several locations along the length of the specimen, as displayed in Fig. 3a. The formwork was arranged between the lateral control steel beams at the ends of the specimen (Fig. 2a), so that concreting could be carried out directly in the test setup. After completion of concreting, the top was closed with formwork (Fig. 3b) and a thermal insulation layer. The 20 cm thick layer with a thermal conductivity of 0.03 W/(m·K) was used to reduce the heat flux to a minimum. During the entire test period of 7 days, both the bottom and the top surfaces of the specimen remained framed and isolated. On the vertical sides of the specimen, the formwork was removed after 1 day (Fig. 3c) and replaced with a thermal insulation containment to introduce controlled ambient temperature and humidity using an air conditioning device. In the anchorage areas, heat flux was prevented by attaching insulation on the side-surfaces.

The active displacement control was realised by sensing the displacement at both ends with linear time-variable displacement sensors (LDTVs). During the first hours of the hardening phase with compressive stress, the LDTVs measured the displacement between the floor and the load introduction adapters on both sides of the specimen. Once sufficient bond developed between the concrete and the threaded steel bars protruding from the specimen at both ends without contact to the load adaptors (Fig. 3a), these LDTVs were repositioned to directly measure the displacement between these bars and the floor (Fig. 3d). This avoided any error due to movements within the load introduction adapter. In response to an infinitesimal change in the longitudinal displacement detected by the LDTVs, the linked hydraulic cylinder actively compensated for this displacement by applying the required compressive or tensile force, keeping the displacement difference between the specimen ends equal to zero.

3.3 Experiment series and varied design parameters

The individual tests were labelled using a nomenclature specifying the full or partial restraint [F|P], the slow, normal, and rapid hydration rate [S|N|R], the reinforcement bar diameter in mm [10|12|14|16], and the height of the specimen in cm [25|50|100]. To assess the significance of the degree of restraint for the early stress development, four specimens were tested
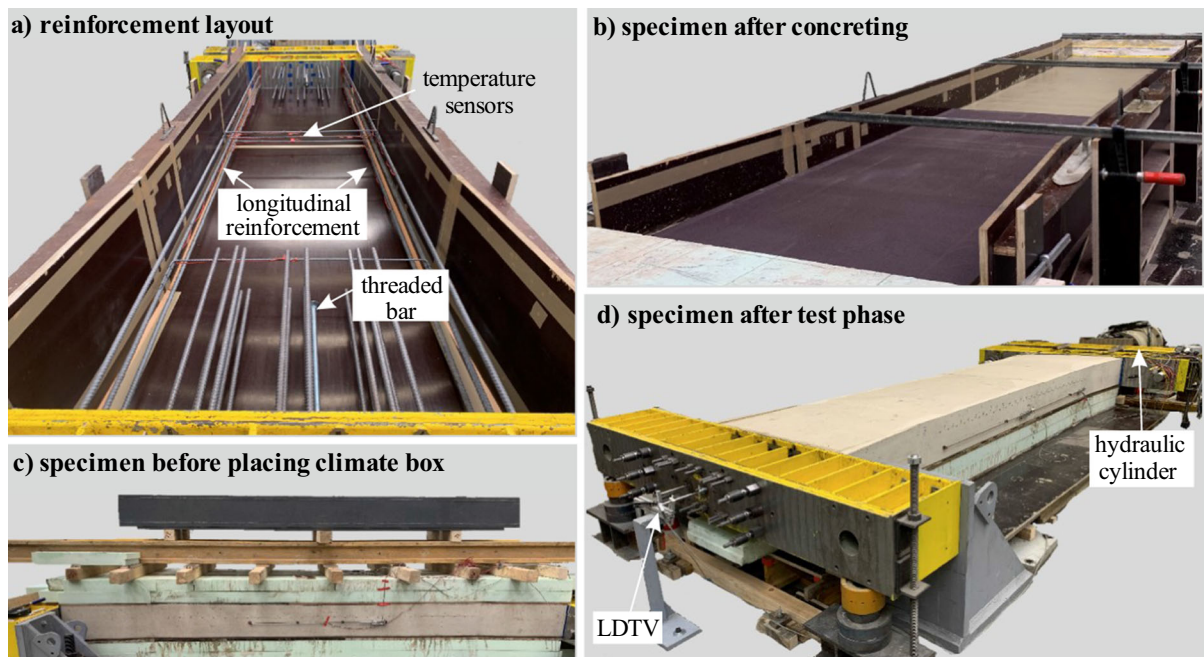

Fig. 3 Different steps of the test procedure from placing the reinforcement in the test setup to the end of the test phase after 7 days, exemplarily shown for a specimen of 1.0 m height

under varying levels of restraint in the first step. Subsequently, the other design-relevant parameters hydration rate, reinforcement ratio and specimen height were tested under fully restrained condition using the described test setup with the active zero displacement control.

The parameters of the three concrete mixtures used are listed in Table 1, the concrete was ready-mixed and transported to the lab. The concrete mixtures were designed to differ in the hydration rate by using different types of cement and fly ash in case of slowly hydrating concrete. To achieve approximately equal compressive strength after 28 days for all concrete mixtures, the water/cement ratio for the rapidly hydrating concrete was changed from 0.45 to 0.55.

The minimum reinforcement ratio was calculated according to Eq. (2), with $w_k = 0.3$ mm, $f_{ct,eff}$ as given in Table 1 assuming early cracking, $\beta = 0.4$ for long-term loading and the effective height h_{eff} as displayed in Fig. 4. All geometrical parameters of the specimens are specified in Table 2. For each parameter combination, two test replications labelled A and B were conducted.

Simultaneously with the restraint tests, material tests were carried out to determine the values of the concrete compressive and tensile strength as well as the compressive Young's modulus at different ages. The values obtained for the cylindrical compressive strength f_c, the centric tensile strength acquired by means of splitting tests with $f_{ct} = 0.9 \cdot f_{ct,sp}$, and the tangential Young's modulus E_c are listed in Table 3. The differences in the days of material testing for the 28-day old concrete were due to lab closures and had no other reason.

The temperature of the fresh concrete T_f remained an uncontrollable influencing factor. Its variations could not be avoided due to the annual temperature
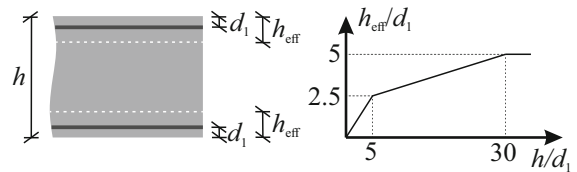

Fig. 4 Calculation of the effective height h_{eff} according to the German National Annex to Eurocode 2 (adapted from [45])

differences occurring throughout the testing phase (see Table 4).

4 Results

4.1 Temperature and restraint-induced stress development

4.1.1 Influence of the degree of restraint

The effect of partially restrained deformation on the induced stress development and crack occurrence was investigated by allowing small longitudinal deformations of the specimens. The degree of restraint was introduced according to [21] as the ratio between the time-dependent cross-sectional stiffness and the equivalent stiffness of the restraint. This equivalent stiffness was quantified as the ratio of the specimen's contraction measured after 7 days with respect to its initial length. For example, the degrees of restraint of 0.18 and 0.20 for the specimens P:N-12-50-A and P:R-12-50-A corresponded to an equivalent stiffness of a restraining frame of 200 MN/m. To achieve a degree of restraint of 0.99 and 0.98, respectively, a frame stiffness of 83,000 MN/m² for specimen P:N-12-50-B and 38 000 MN/m for specimen P:R-12-50-B would be required. These degrees could only be achieved using the active displacement control. The differences in the values of

Table 1 Concrete mixtures of the test specimens

Hydration rate (S/N/R)	Cement type	Cement [kg/m³]	Water [kg/m³]	Fly ash [kg/m³]	Water–cement ratio	$f_{ct,eff}$[a] [MPa]
S (slow)	CEM III/A 42.5 N	310	159	105	0.45	1.5
N (normal)	CEM III/A 42.5 N	360	162	0	0.45	1.5
R (rapid)	CEM I 52.5 R	330	181	0	0.55	1.8

[a]Assuming an early cracking, values used for test design only

Table 2 Geometrical specifications of the test groups

test group	S/N/R	h [m]	l/b [m/m]	c [cm]	d_s [mm]	d_1 [cm]	ρ [%]	h_{eff} [cm]	ρ_{eff} [%]
F:R-10-25	R	0.25	4.5/0.3	3.5	10	4.0	0.63	10.5	0.82
F:S-12-50	S	0.5			12	4.1	0.45	13.2	0.86
P:N-12-50	N	0.5			12	4.1	0.45	13.2	0.86
F:N-12-50	N	0.5			12	4.1	0.45	13.2	0.86
P:R-12-50	R	0.5			12	4.1	0.45	13.2	0.86
F:R-12-50	R	0.5			12	4.1	0.45	13.2	0.86
F:R-14-50	R	0.5			14	4.2	0.62	13.4	1.15
F:R-16-100	R	1.0			16	4.3	0.40	18.6	1.08

h Height; l Length; b Width; c Concrete cover; d_1 Distance surface to centre of reinforcement layout; ρ_{eff} Effective reinforcement ratio calculated acc. to [45]

Table 3 Concrete strength and Young's modulus at different ages as results of material tests

test group	Specimen	Compressive strength f_c [MPa]				Tensile strength f_{ct} [MPa]					Young's modulus E_c [MPa]				
		1 d	2 d	7 d	28 d	1 d	2 d	3 d	7 d	28 d	1 d	2 d	3 d	7 d	28 d
F:R-10-25	-A	26	33	38	42	2.3	2.4	–	2.9	3.9	22,200	24,400	–	26,000	26,600
	-B	23	–	32	39[a]	2.1	–	–	2.0	2.3[a]	21,600	–	–	24,200	26,300[a]
F:S-12-50	-A	10	15	31	43	1.0	1.5	1.4	2.3	2.6	15,400	18,400	21,700	26,400	27,200
	-B	12	21	32	44	1.4	1.7	–	2.7	3.2	15,400	21,000	–	23,600	26,800
P:N-12-50	-A	13	22	36	48	–	–	–	3.0	3.5	18,000	23,100	25,000	26,600	29,100
	-B	13	–	40	59	1.1	–	–	3.2	–	19,400	–	–	28,600	–
F:N-12-50		13	18	34	46	1.4	1.6	2.0	2.2	3.1	18,000	20,700	21,500	27,900	29,200
P:R-12-50	-A	27	32	40	45[a]	2.2	2.7	–	2.7	3.2[a]	20,700	22,400	–	26,200	26,400[a]
	-B	17	24	30	31	1.5	1.8	–	1.9	2.3	–	21,700	–	23,300	–
F:R-12-50		34	39	45	48	2.6	3.2	3.3	3.1	3.3	27,100	27,000	26,300	28,200	28,400
F:R-14-50	-A	24	32	38	42	1.8	2.5	2.6	2.7	2.9	21,300	24,600	25,100	25,600	26,700
	-B	25	32	38	42	2.1	2.3	2.4	2.6	2.7	23,600	24,800	24,900	–	27,100
F:R-16-100	-A	30	37	42	47[b]	1.9	2.9	–	3.2	3.7[b]	25,200	25,500	–	27,100	27,100[b]
	-B	30	35	38	52[a]	2.5	3.0	–	3.0	2.9[a]	23,900	25,200	–	26,500	–

[a]Tested after 27 days; [b]tested after 29 days.

the equivalent stiffness quantified for the two latter specimens are due to different development of the Young's modulus over time. Depending on the stiffness and the hydration rate, the total deformation after 7 days was either 15 μm/m for the stiffness of 200 MN/m or 5 and 7 μm/m for the stiffness of 38,000 MN/m and 84 000 MN/m, respectively.

The performance of these two partial restraint levels was compared to a fully restrained condition,

with a degree of restraint of 1.0, for geometric identical specimens. As Fig. 5 shows, the full restraint led to earlier cracking that occurred at larger values of tensile stress. For partial restrained conditions, cracking occurred only in rapidly hydrating concrete exhibiting a large timespan of about 72 h between the peak and steady-state temperatures.

Specimens with normal hydration rate and lower temperature development compared to the concrete

Table 4 Significant temperatures and restraint-induced stress σ_{rest} with the time of occurrence for all investigated specimens

Test group	Specimen	Fresh concrete temperature	Maximum core temperature			Zero-stress temperature		Time of first primary cracking			Time of second primary cracking		
		T_f [°C]	T_{max} [°C]	$\sigma_{rest,Tmax}$ [MPa]	t_{Tmax} [h]	T_2 [°C]	t_2 [h]	$T_{cr,1}$ [°C]	$\sigma_{rest,cr,1}$ [MPa]	$t_{cr,1}$ [h]	$T_{cr,2}$ [°C]	$\sigma_{rest,cr,2}$ [MPa]	$t_{cr,2}$ [h]
F:R-10-25	-A	18	49	− 1.2	13.8	44	19.5	24	1.4	44.5		–	
	-B	19	50	− 1.3	14.5	46	19.5	23	1.9	93.6		–	
F:S-12-50	-A	21	42	− 0.7	23.7	38	29.4	22	1.8	64.8		–	
	-B	31	53	− 3.2	21.5	43	34.8	36	1.6	44.4	26	1.5	71.0
P:N-12-50	-A	17	41	− 0.4	23.6	38	30.0		–			–	
	-B	14	39	− 0.6	19.0	36	27.0		–			–	
F:N-12-50		22	46	− 0.7	20.9	42	26.3	24	2.0	50.3	–		
P:R-12-50	-A	10	49	− 1.1	23.0	38	37.9		–			–	
	-B	9	49	− 0.6	19.9	45	24.6	23	1.3	101.0		–	
F:R-12-50		16	57	− 2.2	20.5	46	28.5	37	1.9	36.3	19	2.1	72.8
F:R-14-50	-A	9	47	− 2.2	21.6	39	31.6	27	1.9	48.1		–	
	-B	22	56	− 1.7	18.9	43	24.1	41	1.6	32.6	24	1.8	55.4
F:R-16-100	-A	22	65	− 1.3	18.8	63	26.8	57	1.2	36.1	34	1.2	70.9
	-B	20	62	− 2.0	22.0	57	35.4	48	1.2	47.1		–	

with rapid hydration (Fig. 5a) showed cracking only under a fully restrained condition and climate-controlled cooling within the first 7 days, as shown by the restraint-induced stress development for specimen F:N-12-50 in Fig. 5c. No cracking was observed for the other two partially restraint specimens P:N-12-50-A and -B.

Despite having a rapid hydration rate, as for specimen P:R-12-50-A, the restraint-induced stress developing at an allowed deformation of 15 μm/m did not reach the tensile strength, as shown in Fig. 5b, d. When the allowed deformation is reduced to 5 μm/m, as for P:R-12-50-B, or when a fully restrained condition is achieved, as for F:R-12-50, the stress evolution under rapid hydration led to cracking in both specimens. The fully restrained specimen with a controlled environment and a fast-decreasing temperature showed two primary cracks, which occurred after 36 and 73 h, while for the partially restrained

specimen P:R-12-50-B the only crack occurred after 101 h.

4.1.2 Influence of the hydration rate

The hydration rate of the concrete mixture (slow, normal, and rapid) affects the temperature, strength, and Young's modulus development in a specimen, depending on the fresh concrete temperature and ambient temperature and mechanical boundary conditions. Faster hydration leads to faster temperature development with a higher peak value inside the specimen, inducing faster strain and stress development with higher peak values. In parallel, the tensile strength develops faster (see Fig. 6), meaning that a higher restraint-induced stress is necessary for the specimen to crack. As a result, different hydration rates affected the time of cracking, while the restraint-
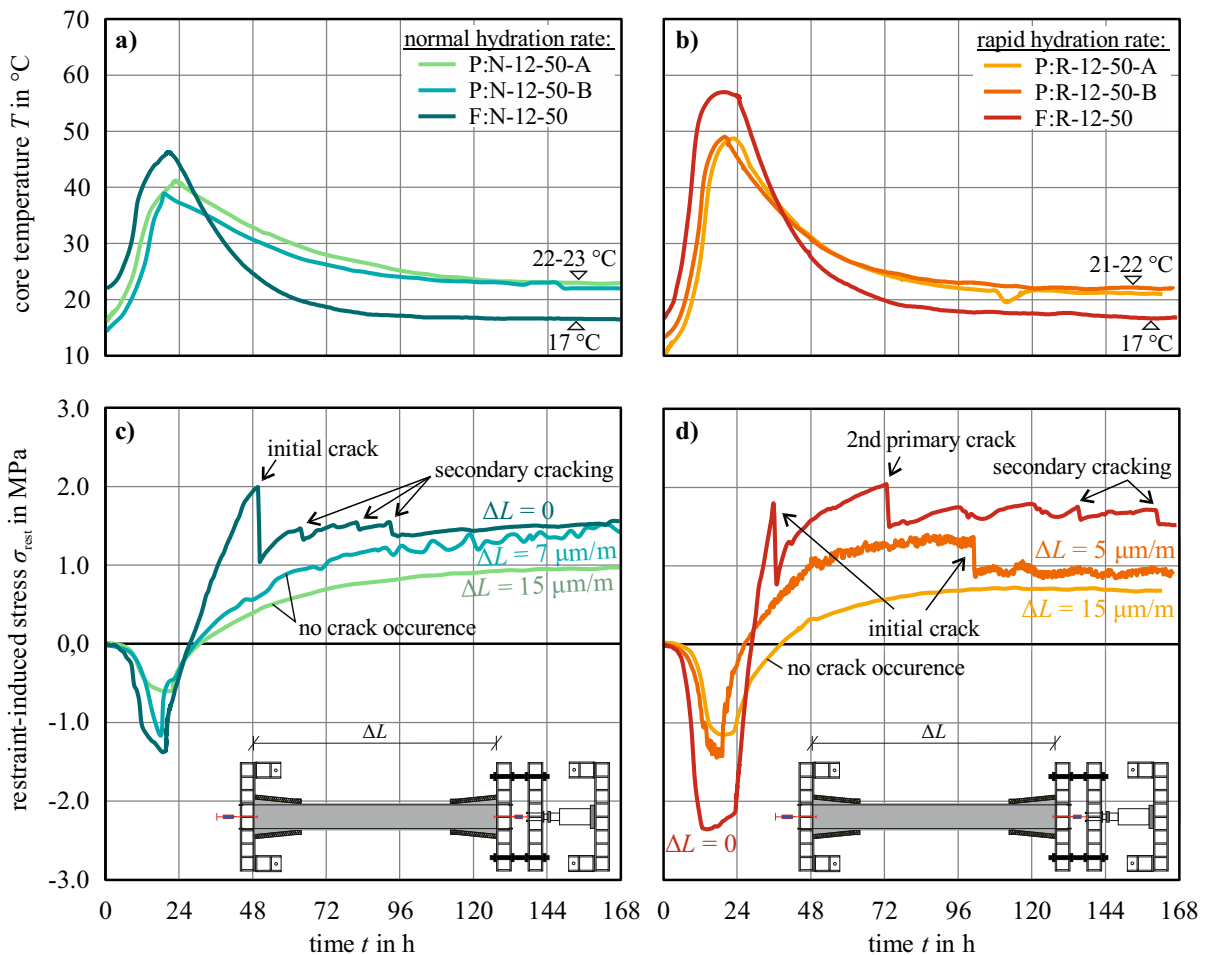
Fig. 5 Temperature development of the partially restrained specimens (P) and the corresponding specimens under full restrain (F) for different hydration rates (**a**, **b**) with the influence on the restraint-induced stress development (**c**, **d**)

induced stress values showed marginal variations at crack occurrence (Fig. 7a, b).

Figure 6 displays the development curves of the compressive strength, tensile strength, and Young's modulus of the three concrete mixtures used in relation to the 28-day value, indicated as ξ_{ct28} for the tensile strength ratio and ξ_{E28} for the Young's modulus ratio. The curves are obtained as the average of the individual strength or Young's modulus values for each specimen from the material tests (see Table 3). In addition, the strength and stiffness development curves according to *fib* Model Code 2010 [46], which are equal to those in Eurocode 2 [44] and the German Annex to Eurocode 2 [45], are plotted as grey dashed lines with a strength development factor of $s = 0.25$

for the slow and normal hydration rate and $s = 0.20$ for the rapid hydration rate.

Regardless of the hydration rate of the concrete mixture, the Young's modulus developed the fastest, followed by the tensile strength, while the compressive strength developed the slowest. The rapidly hydrating concrete mixture exhibited very high strength and stiffness at early ages compared to the other concrete mixtures. To document this, Fig. 6c shows that 80 and 90% of the 28-day values for tensile strength and Young's modulus, respectively, were reached after 2 days. Typically, the usage of fly ash in concrete reduces the strength and Young's modulus development during the first 28 days [53, 54]. This behaviour was not observed in the experimental campaign, as the comparison of the material test data
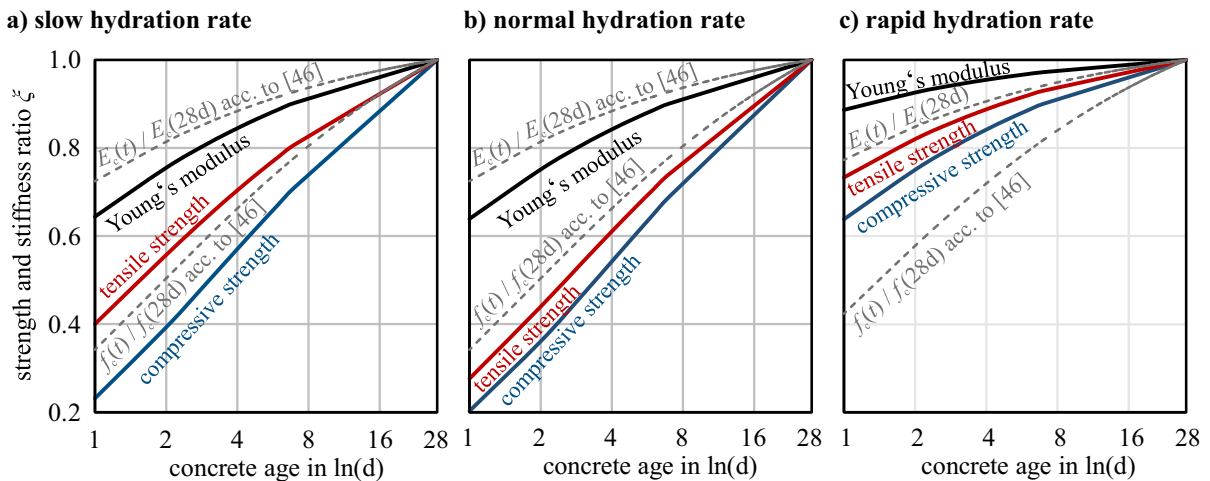
Fig. 6 Average strength and stiffness development for different hydration rates in relation to the 28-day value, taken from material tests. In addition, the development curves according to *fib* Model Code 2010 [46] are depicted as grey dashed lines with a strength development factor of $s = 0.25$ for the slow and normal hydration rate and $s = 0.20$ for the rapid hydration rate

in Fig. 6 shows. No reduction in strength and Young's modulus development was observed for the slowly hydrating concrete compared to the normally hydrating concrete, despite replacing 25% of the cement with fly ash in the slowly hydrating concrete, while the cement type and water–cement ratio remained identical. Furthermore, the tensile strength values compared to the 28-day value were lower for the normally hydrating concrete compared to the slowly hydrating one. Considering the absolute values of concrete properties at the age of 28 days as listed in Table 3, the strength and Young's modulus of concrete with the normal hydration rate are higher than the values for the slow hydration rate. For example, the average compressive strength for the normally hydrating concrete is 51 MPa, which is 7 MPa higher compared to the slowly hydrating one.

The magnitude of the concrete strength and Young's modulus depends on the temperature of the member, as higher concrete temperature affects the pore structure and results in a coarser matrix [55, 56]. This results in a reduced strength and stiffness of concrete under elevated temperature compared to concrete hydrating at temperatures between 20 and 40 °C. Temperature sensitivity is particularly important for high-strength concrete at temperatures above 100 °C [57, 58], and is considered in design codes such as *fib* Model Code 2010 by reducing the strength and Young's modulus for a concrete temperature above 20 °C and below 80 °C (see Sect. 5.1.10 in

[46]). The experimental results, however, do not show a negative influence on the tensile strength or Youngs's modulus, as the following discussion points out.

As the development of the core temperature shows in Fig. 7a, the specimens with slow (F:S-12-50-A) and normal (F:N-12-50) hydration rates followed a similar profile, starting at a fresh concrete temperature of 21–22 °C with a small difference in the peak temperatures of 42 °C and 46 °C, respectively (cf. Table 4). For the rapidly hydrating specimen F:R-12-50 a higher maximum temperature of 57 °C is measured, even for a lower fresh concrete temperature of 16 °C, compared to the two other specimens. After 4 days the cooling phase is finished, reaching the steady-state temperature of 17 °C for all three specimens.

As apparent from the comparison, a larger difference between the fresh concrete and peak temperatures induced larger compressive stress values, as shown in Fig. 7c. Here, the specimen with a rapidly hydrating concrete (F:R-12-50) reached the maximum compressive stress of 2.3 MPa, the normally and slowly hydrating cements exhibited the maximum values of 1.1 MPa for F:N-12-50 and 0.9 MPa for F:S-12-50-A, respectively. While the maximum core temperature has been reached at the same hydration age, i.e. shortly after removing the formwork, for all three specimens the peak of compression was reached at different ages. This difference is owing to the creep and relaxation behaviour of each specimen. A high
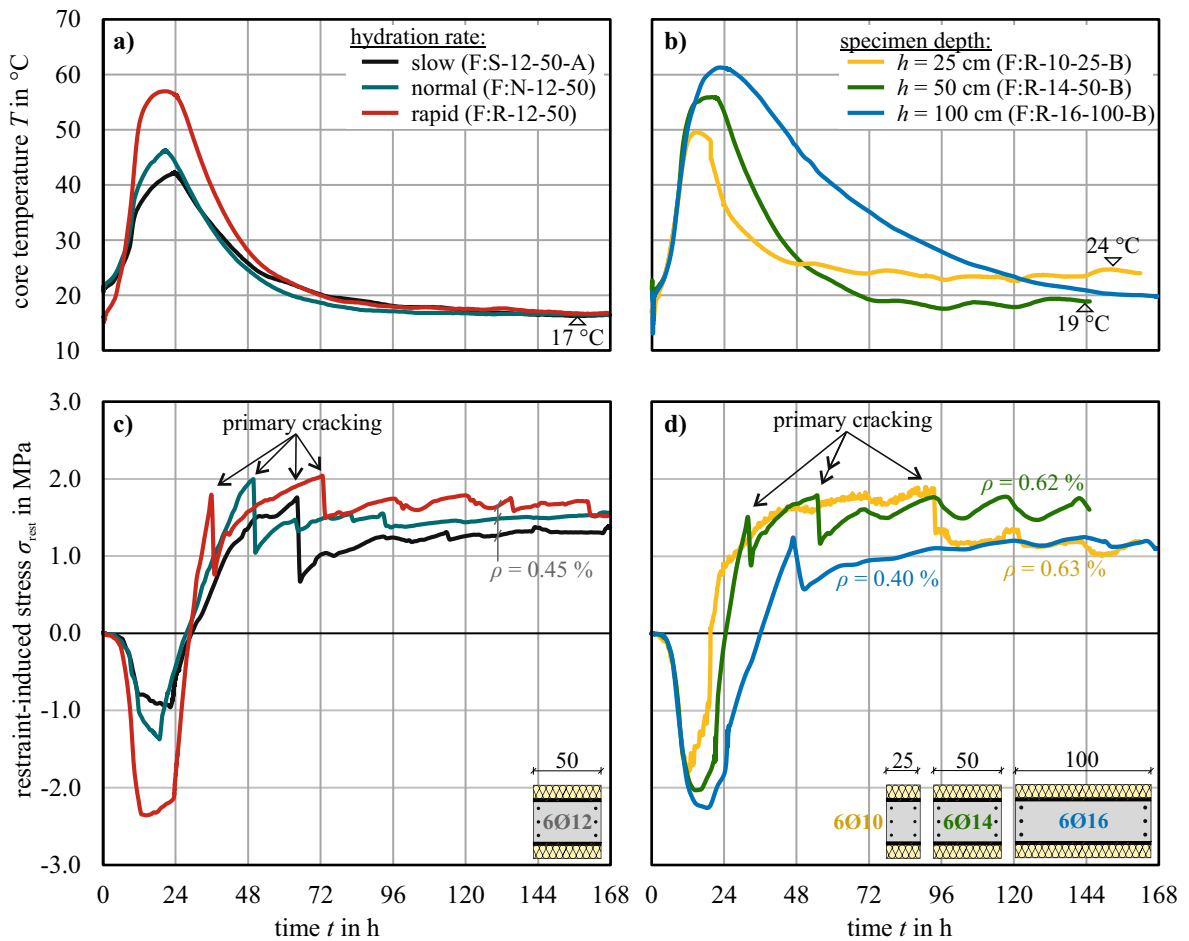
Fig. 7 Temperature development in dependence of the hydration rate (**a**) and the specimen height (**b**) with the corresponding restraint-induced stress development (**c, d**)

temperature gradient within a short time period results in lower amount of creep compared to slower temperature changes over a longer period of time. In addition to the viscoelastic behaviour, the faster hydration and higher concrete temperatures of specimen F:R-12-50 led to an increased shrinkage compared to F:N-12-50 and F:S-12-50-A. As reported e.g. in [15, 16], the magnitude of autogenous and chemical shrinkage is higher with rapid hydration and high concrete temperature, especially in the first days of concrete age. This leads to a superposition of the compressive strain induced by the increasing temperature and the tensile strain induced by the shrinkage, which affects the magnitude and time of the maximum compression in the specimens. A similar effect

increases the total restraint-induced tension as a superposition of a temperature-induced tensile strain due to cooling of the specimens and continuing shrinkage, as with ongoing exposure of the specimens to ambient humidity, drying shrinkage increasingly influences the evolution of the restraint-induced stress.

The comparison of the time of initial cracking provided in Fig. 7c shows that faster hydration and thus a larger temperature drop results in earlier cracking. The rapidly hydrating specimen led to an initial crack after 36 h, whereas the other two specimens cracked after 50 h for the normal hydration rate and after 65 h for the slow hydration rate, respectively. This difference can be related to the evolution profiles of the tensile strength and Young's modulus at early

age displayed in Fig. 6. Apparently, for the rapidly hydrating specimens, the high Young's modulus ratio ξ_{E28} led to an early crack despite the high tensile strength evolving simultaneously to the Young's modulus. For the slowly and normally hydrating concretes with an equally developing Young's modulus ratio ξ_{E28}, the time of initial cracking was influenced by the development of the tensile strength and the different evolutions of the restraint-induced stress. Both the compressive stress and the tensile stress at initial cracking are lower for the slowly hydrating specimen F:S-12-50-A compared to the normally hydrating specimen F:N-12-50, which can be attributed to a slower hydration evolution as shown by the temperature development in Fig. 7a for both specimen.

The stress drop upon crack occurrence is equally high for all three specimens, approximately 1 MPa. Nevertheless, slightly lower restraint stress at cracking seem to increase the stress drop, as the comparison of the specimens F:N-12-50 and F:S-12-50-A show. Because of the early cracking and the high temperature difference between the initial cracking and the steady-state temperature in F:R-12-50, another primary crack formed after 72 h. The stress drop of 0.5 MPa is remarkably lower than the other observed stress drops due to the reduction of the overall member stiffness after the occurrence of the initial crack. No specimen showed additional primary cracks after 96 h, merely because no significant temperature changes occurred anymore.

4.1.3 Influence of the member height

The varied height of the specimen (25 cm, 50 cm, and 100 cm) affects the interaction between the heat flux and the heat generation. Thicker members show a higher temperature value and a longer cooling down phase (Fig. 7b). The larger differences between core and surface temperature in thicker members induce a higher non-linear self-equilibrating stress profile, which added up to the restraint-induced stress provokes cracking at lower restraint-induced stress values as compared to thinner members (Fig. 7d).

As Fig. 7b shows, the core temperatures developed similarly in the first hours for equal concrete mixtures and fresh concrete temperatures of 18–22 °C regardless of the specimen height. The maximum core temperature varied for the individual specimens from 50 °C for the thinnest specimen of 25 cm (F:R-10-25-B) to 56 °C at a thickness of 50 cm (F:R-14-50-B) and

62 °C at 100 cm (F:R-16-100-B). The differences in the temperature development resulted from the interaction of the heat flux and heat generation, affected by the specimen geometry, i.e. by the surface to volume ratio. Therefore, the thicker specimens reached their maximum temperature later and the cooling rate was slower. F:R-16-100-B did not reach the steady-state temperature within the first 7 days. The small temperature fluctuations of F:R-10-25-B and F:R-14-50-B were caused by a hot summer week with very high ambient temperatures throughout the day limiting the effectiveness of the air-conditioned containment.

As shown in Fig. 7d, the uniform temperature raise at the beginning resulted in a uniform increase in compressive stress for all three specimens, with creep affecting all imposed strains equally. The higher peak temperature reached in the thick specimen (F:R-16-100-B) induced the maximum compression of 2.2 MPa, which is by 0.5 MPa higher compared to the thin specimen (F:R-10-25-B). For the latter, the initial crack occurred the latest of all three specimens, after 94 h. In the thickest specimen, the initial crack occurred at a tensile stress of 1.2 MPa, being significantly lower compared to all other five specimens. Apparently, the high self-equilibrating stress profile occurring in thick members and adding up to the restraint-induced stresses was of significant relevance for the time and stress level of crack formation.

4.1.4 Influence of the reinforcement ratio

In an uncracked member, the influence of the reinforcement is of subordinate significance for the time of initial cracking and the corresponding restraint-induced stress value (Fig. 7c, d). After cracking, the reinforcement ratio influences the crack opening and the stiffness of the cracked member. A higher reinforcement ratio results in a lower stress drop due to cracking.

For the geometrically identical specimens F:R-14-50-B ($\rho = 0.62\%$) and F:R-12-50 ($\rho = 0.45\%$), both with the same concrete mixture, initial cracks appeared at around the same time after about 30 h. However, the higher reinforcement ratio of F:R-14-50-B resulted in a lower stress drop of 0.5 MPa compared to 1.5 MPa for F:R-12-50. The second primary crack occurred 17 h earlier for F:R-14-50-B than for the lower reinforced specimen due to a faster increasing stress. The reason for this was the higher

stiffness of the cracked member. Both specimens showed a similar value of stress drop of approximately 0.5 MPa at occurrence of the second primary crack.

4.2 Crack formation

The crack behaviour and crack formation in the specimens is affected by the effective height of the reinforcement in relation to the specimen height, as documented by the crack patterns shown in Fig. 8. For

the thin members ($h = 25$ cm, F:R-10-25) with an effective height h_{eff} of 10.5 cm on each side of the longitudinal reinforcement, only a single primary crack occurred in each specimen. A larger difference in the ratio of effective height to specimen height led to the development of secondary cracks. Thus, in members of 50 cm height ($h_{eff} \sim 13$ cm) secondary cracks occurred around a primary crack. For the thickest members ($h = 100$ cm, $h_{eff} = 18.6$ cm) a pronounced secondary crack pattern was observed
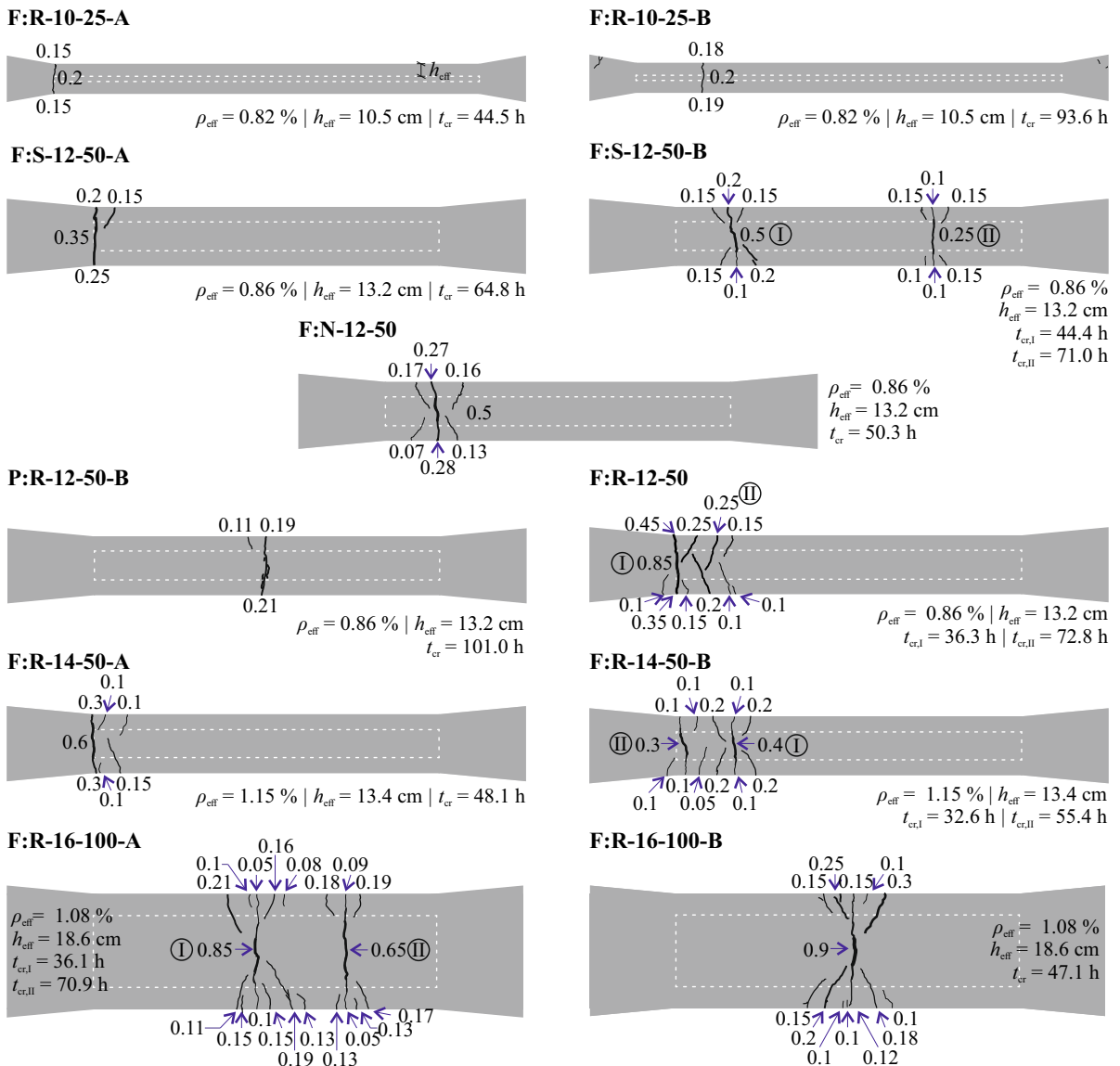
Fig. 8 Crack formation in the specimens with corresponding crack widths measured after 7 days and their effective height of the reinforcement h_{eff} (white dashed lines)

around all primary cracks. Similar observations were reported and discussed in [3, 4, 7]. The length of the secondary cracks in members of 50 to 100 cm height occasionally extended beyond the effective height of the reinforcement calculated according to design in [45]. In all configurations tested, either one or two primary cracks occurred without direct correlation to the design parameters, i.e. concrete mixture and reinforcement ratio.

The transformation of the stress field from a homogeneous to a concentrated tensile stress in the area of the activated reinforcement after the formation of the primary crack causes an inclination of the secondary cracks towards the corresponding adjacent primary crack [3]. Furthermore, the sum of all corresponding crack widths at the specimen side is approximately equal to the crack width of the primary crack in the specimen core. Depending on the amount of the restrained deformation, more secondary cracks are needed to compensate for the deformation imbalance. This effect is particularly pronounced when two inclined secondary cracks occurring simultaneously on opposite sides overlap, as observed in specimen F:R-12-50 for the cracks marked II in Fig. 8. The result is a significant stress drop of similar magnitude to the primary cracks as depicted in Fig. 7c.

Overall, all measured crack widths were equal to or below the limit value of 0.3 mm defined in design codes [44–46], except for the initial crack for specimen F:R-12-50 with a crack width of 0.35 mm and 0.45 mm, respectively. Of the total of 134 cracks detected, only 1.5% exceeded the design limit.

Theoretically, as secondary cracking progresses, the magnitude of the released force and the associated steel stress increment decreases upon each crack occurrence. Consequently, the crack width of each newly occurring crack should get smaller and the length of secondary cracks shorter. At the same time, the crack width of existing cracks should decrease [48, 59]. This behaviour, illustrated as case 1 in Fig. 9, could be confirmed for specimens where the width of the secondary cracks was smaller than the width of the adjacent primary crack, e.g. in F:N-12-50. However, this scenario does not hold for specimens where the width of some secondary cracks became larger than the width of the primary crack, e.g. in F:R-16-100-A and -B. As case 2 in Fig. 9 illustrates, this situation occurs when a larger secondary crack formed around the first primary crack before sufficient restrained deformation was reached to provoke another primary crack. To conclude, the critical crack width does not necessarily appear at the primary crack so secondary cracks must also be accounted for in the design concept for minimal reinforcement.
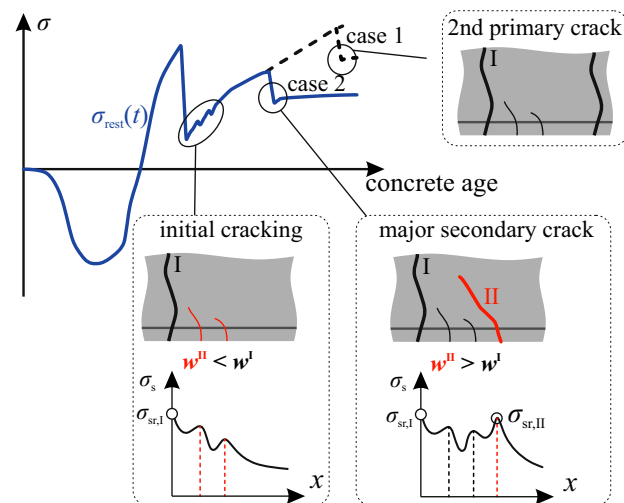

Fig. 9 Qualitative representation of the crack formation with the corresponding steel stress over the reinforcement length x

4.3 Reinforcement stress development and local deformations

In the initial phase of hydration, the tensile stress in the reinforcement changes in response to the compressive stress developing in the concrete member, as Fig. 10 shows. Once the concrete stress turns into tension, the reinforcement in an uncracked section exhibits compression, as documented by the blue curves in the last row of Fig. 10, labelled e and f. Apparently, the changes in reinforcement stress mirror the restraint-induced stress development in concrete and thus counteract the imposed concrete strains in uncracked sections. However, within the stress transfer length of a crack, the reinforcement stress changes sign from compression to tension.

For two specimens (F:S-12-50-B and F:R-16-100-A) these influences of crack formation on local displacements and reinforcement stresses are now investigated in detail. LDTVs attached to both sides of the specimens measured the displacement at the surface. Despite the overall zero deformation of the
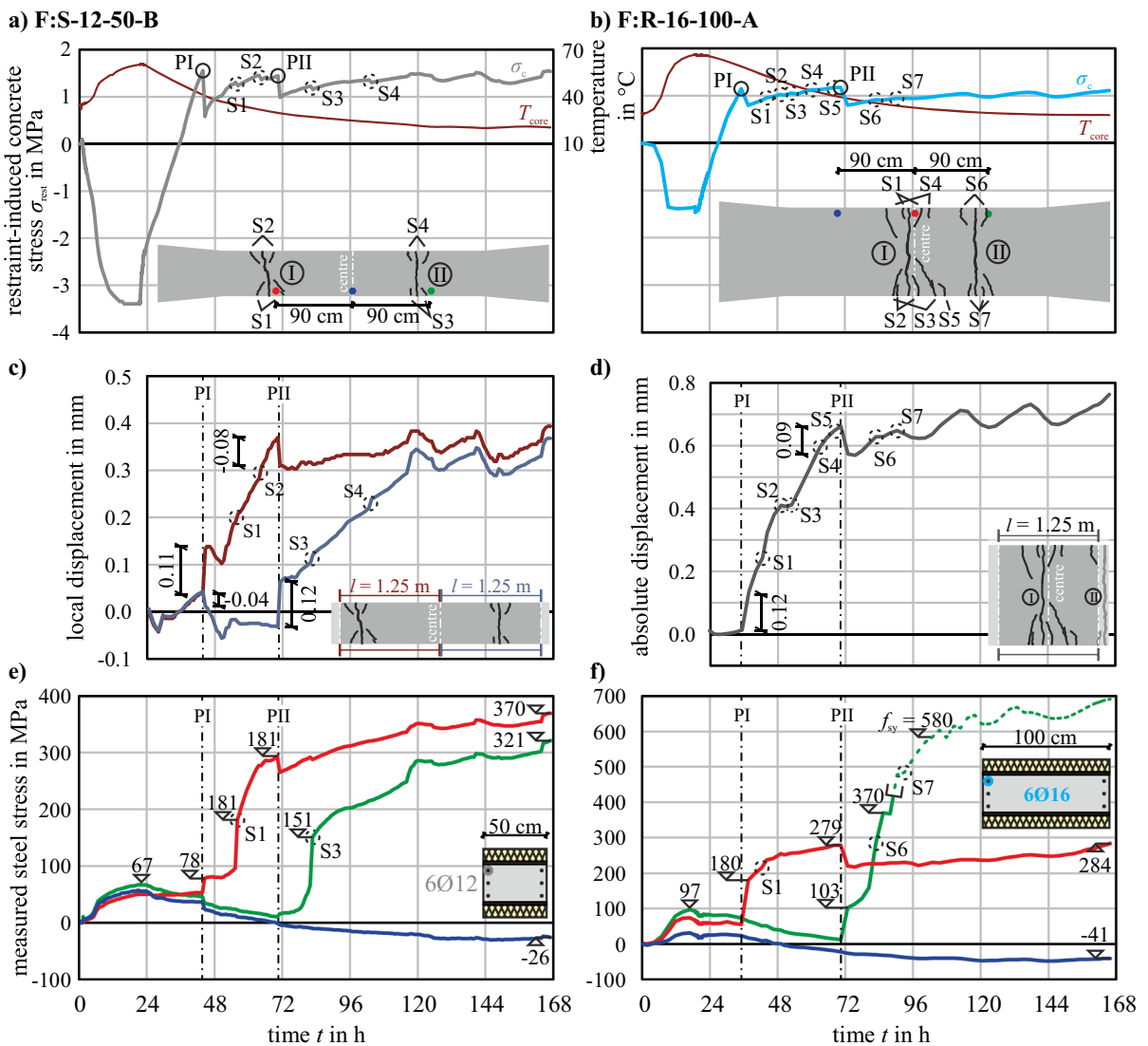
Fig. 10 Evaluation for specimens F:S-12-50-B and F:R-16-100-A: developments of the restraint-induced stress and core temperatures (**a**, **b**), absolute displacements over the test length (**c**, **d**), measured steel stresses at three different locations (**e**, **f**)

specimen, an inhomogeneous stiffness profile along the specimen resulting from the cross-sectional changes in the anchorage region and from cracking allowed for local relative displacement documented by the LDTV measurements shown for the two discussed specimens in the second row in Fig. 10. Upon the occurrence of the primary cracks, the elongation in the adjacent regions increased by around 0.1 mm, while it decreased on the other side of the specimen. Subsequently, the elongation in the cracked section decreased slightly in F:S-12-50-B under increasing restraint-induced stress, which can be attributed to the relaxation of the concrete under the instantaneous stress release after cracking.

Secondary cracking occurred at different times and separately for each side of the specimens. For the thicker specimen, the displacements were approximately twice as high as for F:S-12-50-B, while the average width of all cracks was equal (cf. Fig. 8). In general, the effect of the crack opening of secondary cracks immediately after cracking on the elongation was very small.

The steel stress measured at fixed locations near the first primary crack (green lines in Fig. 10e, f), increased to 78 MPa at a distance of 40 mm after 44 h from the primary crack (F:S-12-50-B) and to 180 MPa at a distance of 52 mm after 36 h for F:R-16-100-A, respectively, both within the stress transfer length. As the width of the primary crack increased continuously, the steel stress increased correspondingly.

A significant increase in reinforcement stress was observed at strain measuring points placed on the steel bars close to a crack, such as in specimen F:S-12-50-B at secondary cracks marked S1, indicated by a red dot in the crack picture of Fig. 10a and a red line in Fig. 10e, and marked S3, indicated by a green dot and green line. Or directly at a crack marked S6 for specimen F:R-16-100-A, indicated by red dot in Fig. 10b and red line in Fig. 10e. While the values of the steel stress directly after the occurrence of the secondary cracks marked S1 and S3 in F:S-12-50-B were between 150 and 180 MPa, the stress increased up to 370 MPa after the occurrence of the crack marked S6 in F:R-16-100-A (green dot and line). For the latter, the ongoing crack opening even led to yielding of the reinforcement, which did not correspond to the observed crack width of about 0.3 mm.

Here, the measuring device apparently failed after this crack opened.

5 Discussion of design-relevant aspects

5.1 Tensile strength and self-equilibrating stress state

The force released upon cracking equals the restraint-induced stress accumulated over the cracked concrete cross-section. As apparent from the above discussion, the stress profile is non-uniform over the cross-section. To provide simple design criteria, an assumption of correspondence between a uniform value of an effective restraint-induced stress and the concrete tensile strength at the time of cracking is often proposed in form of Eq. (1), e.g. in [44–46].

For the conducted test series, a comparison between the actually measured restraint-induced stress at primary cracking $\sigma_{\mathrm{rest,cr}}$ displayed in Table 4 and the tensile strength derived from material tests displayed in Table 3 show, that the restraint-induced stresses are of lower value compared to the tensile strengths. Reasons are potential variations in the tensile strength of concrete, uncertainties in the material test, and mainly the occurrence of the non-linear self-equilibrating stress profile. The latter influences the time of primary crack occurrence depending on the member height without affecting the value of the restraint-induced stress.

To investigate the influence of the self-equilibrating stress profile analytically, a quotient $k \leq 1$ is introduced, similar to the proposal in Eurocode 2 [44], to express the relation between the restraint-induced stress and the tensile strength at the time of primary crack occurrence in the form

$$\sigma_{\mathrm{rest}}(t_{\mathrm{cr}}) = k \cdot f_{\mathrm{ct}}(t_{\mathrm{cr}}). \tag{3}$$

In Eurocode 2 [44] a negligible influence of self-equilibrating stresses on the crack initiation is assumed for thin members ($h \leq 300$ mm) with $k = 1.0$. In contrast, in the German Annex to Eurocode 2 [45] the effect of a self-equilibrating stress profile is taken into account by setting $k = 0.8$ for thin members with an height $h \leq 300$ mm and $k = 0.5$ for $h \geq 800$ mm (cf. [49, 60]).

The estimation of the tensile strength $f_{ct}(t_{cr})$ at cracking is obtained by calculating the strength development according to [44–46].

$$f_{ct}(t_{cr}) = \exp\left[s \cdot \left(1 - \sqrt{\frac{28}{t}}\right)\right] \cdot f_{ct,28d},\qquad(4)$$

where the coefficient s is identified using linear regression to fit the time evolution of the concrete tensile strength specified in Table 3. In [46] the value of factor s is specified according to the hydration rate, with a low value of s being appropriate for rapid hydration. Depending on the cement type used, the strength development factor s can be obtained according to [44–46], e.g. for high strength cement of strength class CEM 52.5 R $s = 0.2$, whereas for normally hydrating cement of class CEM 42.5 N $s = 0.25$. With the factor s derived individually for each specimen, the tensile strength at the time of initial cracking $f_{ct}(t_{cr})$ can be approximated. Once the primary cracks occurred, all self-equilibrating stresses in this cross-section are zeroed and should not be considered when focusing on the secondary cracks [48]. Therefore, only the influence of self-equilibrating stress on primary crack initiation is discussed further on.

The tensile strength at the time of primary cracking $f_{ct}(t_{cr})$ calculated with the determined strength development factor s is compared with the tensile strength $f_{ct,eff}(t_{cr})$ assumed by design codes [44, 46] according to the strength class of the cement in Fig. 11a. To identify whether the tensile strength obtained in the tests is above, below, or equal to the design tensile strength, a dashed diagonal line is added in Fig. 11a. For the three specimens P:R-12-50-B, F:N-12-50 and F:R-16-100-B, the design values fit well with the test data, while the general trend of the data indicates, that the concrete tensile strength is higher than the assumed strength in the design codes.

Because the tensile strength at the time of cracking is used in [44–46] to calculate the force released upon cracking, a higher tensile strength value results in a higher force and increases the amount of reinforcement designed to limit the crack width. Therefore, if a member is assumed to have a lower tensile strength than its actual strength at the time cracking, the calculated reinforcement is not sufficient to limit the crack width according to the design codes.

To give additional insight into the strength development of the specimens, the strength development factor s quantified for all specimens is depicted in Fig. 11b. Comparing the strength development with the design values of 0.25 and 0.2, respectively, assumed in [44–46], the strength development was indeed faster. One explanation is, that the faster development of the tensile strength in relation to the compressive strength (see also Fig. 6), to which most design codes are calibrated, is not

a) Tensile strength at cracking

b) Influence of member height
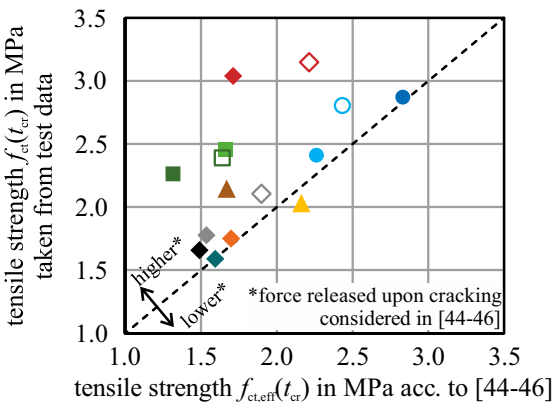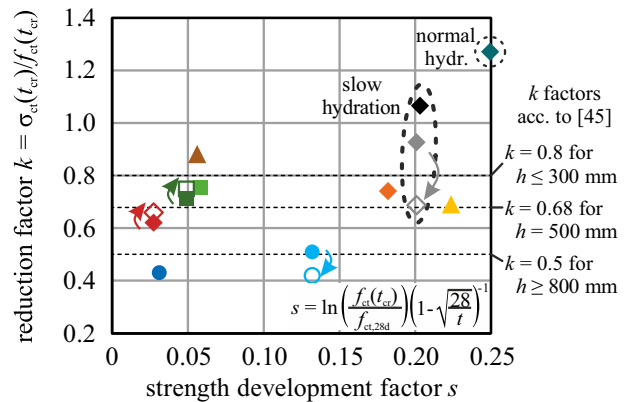
F:R-10-25-A | F:S-12-50-A | P:R-12-50-B | F:R-12-50 | F:R-14-50-A | F:R-16-100-A
F:R-10-25-B | F:S-12-50-B | F:N-12-50 | 2nd primary crack / 1st primary crack | F:R-14-50-B | F:R-16-100-B

Fig. 11 **a** Tensile strength $f_{ct}(t_{cr})$ calculated with Eq. (4) at the time of primary cracking using the adjusted strength development factor s obtained from material test compared to the calculated tensile strength $f_{ct,eff}(t_{cr})$ using the design values from [44–46]; **b** Ratio of self-equilibrating stress expressed by a reduction factor k at the time of cracking to the strength development factor s

adequately represented. Similar observations are reported, suggesting to assume higher strength values for early age concrete [61, 62].

In addition to the tensile strength at cracking, the member height and the self-equilibrating stress profile is of interest. Significant influence of self-equilibrating stress is shown in Fig. 11b for specimens with a rapidly hydrating concrete by the lower reduction factor k for a decreasing strength development factor s. One reason is, that due to the high temperature difference over the cross-sectional height, the magnitude of the self-equilibrating stress increased and provoked earlier cracking.

The reduction factor of the specimens with a rapid hydration fit well with the proposed k-factors according to the German Annex to Eurocode 2 [45] for members of 500 mm height h and a proposed $k = 0.68$ and for a height of more than 800 mm and a proposed $k = 0.5$, as shown by the dashed lines in Fig. 11. For the slowly and normally hydrating specimens, the reduction factor calculated for the first primary crack is significantly above the design value of $k = 0.68$ for the 500 mm thick specimens and ranges from $k = 0.93$ for specimen F:S-12-50-B to 1.27 for specimen F:N-12-50,respectively. This concludes that the influence of self-equilibrating stress is of minor or no significance for the crack induction for the slowly and normally hydrating specimens.

In the case of a second primary crack, the influence of self-equilibrating stresses was even higher for specimen with a slow hydration rate (F:S-12-50-B, grey) or a high height (F:R-16-100-A, light blue) than at initial cracking, as indicated by a lower value of k in Fig. 11b. For both, the second primary crack occurred after 71 h and the restraint-induced stress was ~ 0.1 MPa lower compared to the initial crack (cf. Table 4). On the other hand, the opposite was observed for the rapidly hydrating specimens (F:R-12-50, red marker and F:R-14-50-B, dark green), where the influence of the self-equilibrating stresses onto the restraint-induced stress at second primary crack was slightly reduced.

To conclude, the tensile strength development for concrete members should be assumed to be faster than proposed by the design codes in [44–46]. Especially for rapidly hydrating concrete, high strength values can occur at early ages. While the large influence of self-equilibrating stress on thicker members under rapid hydration is well accounted for in [45], the influence of self-equilibrating stress on the slowly and

normally hydrating specimens is negligible. Both, the assumed higher strength values at cracking and the missing influence of self-equilibrating stress, expressed by $k = 1.0$, indicate larger forces released upon cracking. Thus requiring more reinforcement to limit the crack width when using the design approaches in [44–46]. On the other hand, the crack widths measured after 7 days show, that the limitation of 0.3 mm is sufficiently complied with for the reinforcement layout used, which was calculated with $f_{ct,eff}$ according to Table 1 and $k = 0.68$. Only in specimen F:R-12-50 the first primary crack exceeded the limit, which fits to the observations made in Fig. 11 with a high tensile strength at the time of cracking, while the influence of self-equilibrating stress agrees well with the design code.

5.2 Steel stresses and bond strength at primary cracking

To investigate the influence of reinforcement and bond on the crack width, a study on steel stress and bond strength at the occurrence of primary cracks is conducted. In order to relate the measured values of steel stress to the assumptions in *fib* Model Code 2010 [46] and in Eurocode 2 [44], the concept of design bond strength τ_{bm} was adopted in the evaluation shown in Fig. 12. The dashed curves in Fig. 12a show the steel stress profiles corresponding to the values of different design bond strengths τ_{bm} in relation to the bar diameter Ø. The values of steel stress in the individual cracks depicted in Fig. 12a were obtained by considering the restraint-induced force immediately after the crack occurrence, with the crack opening releasing deformation and reducing the restraint-induced stress.

As apparent from Fig. 12a, the primary crack width was below 0.16 mm in all cases except for specimen F:N-12-50. The steel stress ranged from 111 MPa for F:R-14-50-A with a crack width of 0.11 mm to 339 MPa for the second primary crack of F:R-12-50. Compared to the crack width limitation of 0.3 mm proposed in [44–46], the crack widths of all primary cracks immediately after occurrence are below this value.

The steel stress profiles corresponding to different design bond strengths indicate a large scatter of bond strength of the specimens, resulting in different steel stress for almost identical crack widths. Consequently, a calculation of a design steel stress to determine the
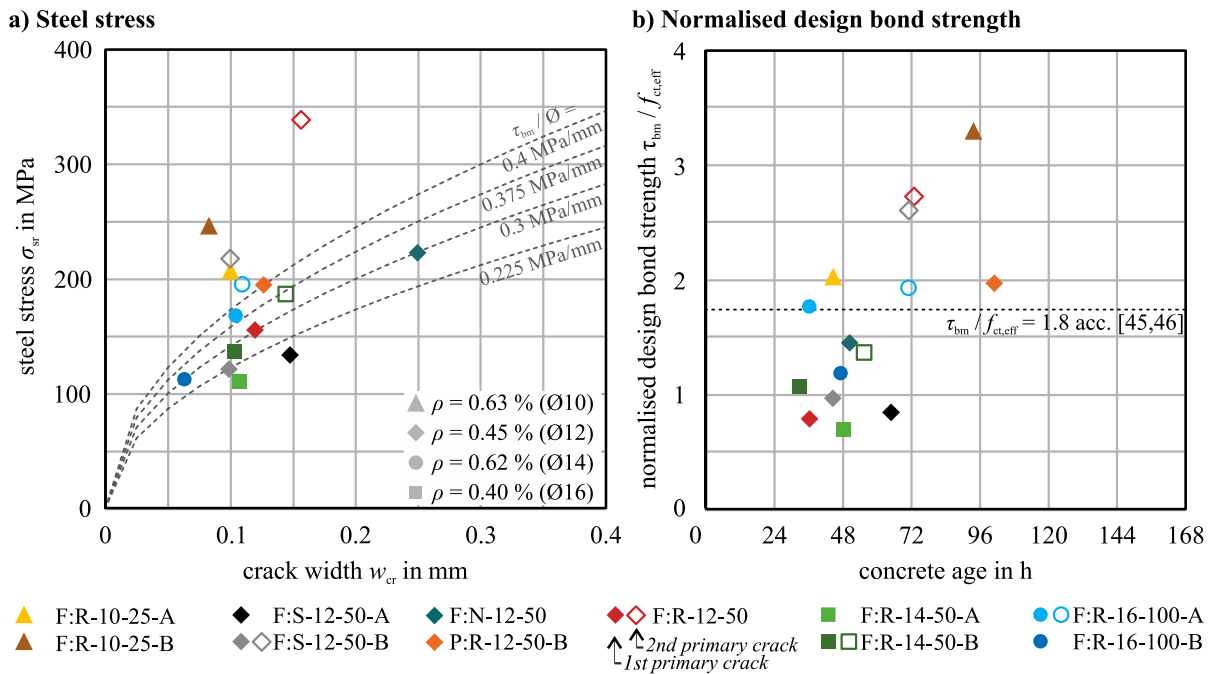
a) Steel stress

b) Normalised design bond strength

Fig. 12 Reinforcement stress in relation to **a** crack width and **b** normalised bond strength at time of cracking

reinforcement for crack width limitation is difficult for an assumed design bond strength.

The design bond strength used in the above evaluation was based on the assumption of a constant stress profile over the transfer length. To obtain its value, Eq. (2) was rearranged to

$$\tau_{bm} = \frac{\sigma_{sr}^2 \cdot d_s \cdot (1 - \beta)}{2 \cdot w_{cr} \cdot E_s \cdot \rho \cdot \alpha_e}. \tag{5}$$

The coefficient β is set to 0.6 for instantaneous loading as suggested in Table 7.6–2 in [46].

Comparing the bond performance at the time of cracking of the specimens with each other is influenced by the time-dependent evolution of Youngs' modulus and strength. To factor out the effect of strength development, a normalised value for the design bond strength was introduced in Fig. 12b as the ratio of the design bond strength provided in Eq. (5) to the time-dependent concrete tensile strength given in Eq. (4). The observations based on Fig. 12a show a link between the bond strength and the concrete age, therefore in Fig. 12b the normalised design bond strength is set in relation to the time of cracking.

The individual values in Fig. 12b indicate that the normalised design bond strength is of low value at a

concrete age of less than 72 h and increases significantly after an age of 3 days. This is consistent with the observations in Fig. 12a, where a low value of steel stress was identified for some specimen. Design bond strength with low value results in a larger crack opening when using design equations such as Eq. (2). Contrary, the crack widths measured immediately after primary cracking are of small value. Furthermore, for most cracks, the crack width limitation of 0.3 mm was satisfied at 7 days of concrete age, assuming that the bond strength at later ages was above the normalised design bond strength $\tau_{bm}/f_{ct}(t_{cr}) = 1.8$, as also shown by the data in Fig. 12b.

As apparent from Eq. (5) and quantitatively documented in Fig. 12b, the normalised design bond strength depends on the crack width. In the codes, however, the design bond strength is assumed constant and linked to the concrete tensile strength, e.g. $\tau_{bm} = 1.8\, f_{ct,eff}$ in [46]. In view of the data evaluated in Fig. 12b, this normative assumption is close to the average value of $\tau_{bm}/f_{ct,eff}$ of the test data, being 1.64. The high scatter of the individual values does not allow any conclusion on an appropriate approximation of the design bond strength as a function for the tensile strength at an early age.

6 Summary

The presented experimental campaign investigated the influences of the degree of restraint, the hydration rate, the member height and the reinforcement ratio of concrete slabs under controlled thermal and mechanical boundary conditions. To ensure reproducible results under well-defined conditions, a new test setup with an actively controlled restrained zero deformation and stable ambient conditions has been developed. The results of the study with systematically varied test and design parameters can be summarised as follows:

- Under fully restrained conditions, the induced stress evolution in the 4.5 m long specimens always led to cracking in the first 7 days, despite differences in their hydration behaviour and cross-sectional area. Tests in which only a small deformation of the specimen between 15 and 5 μm/m was allowed did not show sufficient stress for early cracking. Therefore, the degree of restrained deformation is of high significance for an early crack occurrence.

- While the hydration rate significantly affected the restraint-induced stress evolution, the actual stress value at the time of cracking was nearly equal for members of identical height. Using a concrete mixture with a lower hydration rate delayed the time of initial cracking and significantly reduced the influence of the self-equilibrating stress field on the tensile stress in the member.

- The tensile strength and Youngs' modulus development in the investigated members is faster than the projection done in common design codes, e.g. *fib* Model Code 2010 or Eurocode 2. This means higher restraint-induced stress and a larger released force at crack occurrence compared to the normatively calculated force need to be considered. It is advisable to assume a concrete tensile strength of at least 70 to 90% of the mean tensile value f_{ctm} for early cracking within the first 3 days.

- While the specimens showed a low design bond strength at primary cracking up to a concrete age of 3 days, the bond strength significantly increased for later ages. The normalised design bond strength $\tau_{bm}/f_{ct}(t_{cr}) = 1.8$ proposed in *fib* Model Code 2010 is applicable on average for cracking in the first 7 days, even though higher normalised bond strengths were observed after 3 days.

- Specimens with an effective height ratio h_{eff}/h below 0.53 showed secondary crack occurrence, which reduced the average crack width. As a result, only 1.5% of all cracks detected in all tests had a width above the design limit of 0.3 mm. Therefore, the reinforcement design in the tests was capable to limit the crack widths and ensure serviceability for early cracking.

- Excessive secondary cracking in specimens with an effective height ratio below $h_{eff}/h = 0.37$ reduced the primary crack widths to small values below 0.2 mm. The secondary cracks gradually occurred at each side of the primary crack. Upon the occurrence of a second primary crack, secondary cracks only formed in its vicinity. The largest crack width did not always occur at the primary crack, in some cases a secondary crack showed a slightly larger width.

The presented test setup allows for an investigation under well-defined boundary conditions for a broad range of varying design parameters. The obtained experimental results provide an ideal basis for a deeper, rigorous theoretical interpretation using a coupled hydration-fracture finite-element model.

Declarations

Conflict of interest The authors declare that they have no conflict of interest.

References

1. Carlson RW (1938) Temperatures and stresses in mass concrete. ACI J Proc. https://doi.org/10.14359/8464

2. Townsend CL (1965) Control of temperature cracking in mass concrete. 34, vol 20, Washington DC

3. Helmus M (1990) Mindestbewehrung zwangsbeanspruchter dicker Stahlbetonbauteile. DAfStb-Heft 412. Beuth Verlag GmbH, Berlin

4. Maurer R, Tue NV, Haveresch K-H et al (2005) Mindestbewehrung zur Begrenzung der Rissbreiten bei dicken Wänden. Bauingenieur 80(10):479–485

5. Henning W (1987) Zwangrissbildung und Bewehrung von Stahlbetonwänden auf steifen Unterbauten. Doctoral Thesis, Technische Universität Braunschweig

6. Schütte J (1997) Einfluß der Lagerbedingungen auf Zwang in Betonbodenplatten. Doctoral Thesis, Technische Universität Braunschweig

7. König G, Tue NV (eds) (1996) Grundlagen und Bemessungshilfen für die Rißbreitenbeschränkung im Stahlbeton und Spannbeton sowie Kommentare, Hintergrundinformationen und Anwendungsbeispiele zu den Regelungen nach DIN 1045, EC2 und Model Code 90. DAfStb-Heft 466. Beuth Verlag GmbH, Berlin

8. De SG, Taerwe L (1996) Degree of hydration-based description of mechanical properties of early age concrete. Mater Struct 29:335–344

9. Emborg M (1989) Thermal Stresses in Concrete Structures at Early Ages. Doctoral Thesis, Lulea University of Technology

10. De SG (2002) Fundamental study of early age concrete behaviour as a basis for durable concrete structures. Mat Struct 35(1):15–21. https://doi.org/10.1007/BF02482085

11. Breitenbücher R (1990) Investigation of thermal cracking with the cracking-frame. Mater Struct 23:172–177

12. Springenschmid R (ed) (1994) Thermal cracking in concrete at early ages. CRC Press

13. Weiss WJ, Yang W, Shah SP (1998) Shrinkage cracking of restrained concrete slabs. J Eng Mech 124(7):765–774. https://doi.org/10.1061/(ASCE)0733-9399(1998)124:7(765)

14. Gilbert RI (2001) Shrinkage, cracking and deflection—the serviceability of concrete structures. Electron J Struct Eng 1(1):15–37

15. Altoubat SA, Lange DA (2001) Creep, shrinkage, and cracking of restrained concrete at early age. ACI Mater J 98(4):323–331. https://doi.org/10.14359/10401

16. Holt E, Leivo M (2004) Cracking risks associated with early age shrinkage. Cem Concr Compos 26(5):521–530. https://doi.org/10.1016/S0958-9465(03)00068-4

17. Schmidt C, Bollin M, Cramer J et al (2021) Untersuchungen zur Rissbildung in durchgehend bewehrten Betonfahrbahnen. Bauingenieur 96(10):358–375. https://doi.org/10.37544/0005-6650-2021-10-56

18. Meier A (2012) Der späte Zwang als unterschätzter - aber maßgebender - Lastfall für die Bemessung. Beton- und Stahlbetonbau 107(231):216–224. https://doi.org/10.1002/best.201100085

19. Zou D, Liu T, Teng J et al (2014) Influence of creep and drying shrinkage of reinforced concrete shear walls on the axial shortening of high-rise buildings. Constr Build Mater 55:46–56. https://doi.org/10.1016/j.conbuildmat.2014.01.034

20. Zhu H, Hu Y, Li Q et al (2020) Restrained cracking failure behavior of concrete due to temperature and shrinkage. Constr Build Mater 244:118318. https://doi.org/10.1016/j.conbuildmat.2020.118318

21. Schlicke D, Tue NV (2013) Consideration of viscoelasticity in time step FEM-based restraint analyses of hardening concrete. JMP 04(10):9–14. https://doi.org/10.4236/jmp.2013.410A2002

22. Jin C, Schmidt C, Chudoba R et al (2020) Experimentelle Untersuchungen zur Rissbildung in Stahlbetonbauteilen infolge Zwangbeanspruchung. Beton- und Stahlbetonbau 115(11):906–916. https://doi.org/10.1002/best.202000014

23. Schlicke D (2014) Mindestbewehrung für zwangbeanspruchten Beton. Festlegung unter Berücksichtigung der erhärtungsbedingten Spannungsgeschichte und der Bauteilgeometrie. Doctoral Thesis, Technische Universität Graz

24. Barre F, Bisch P, Chauvel D et al. (2016) Control of cracking in reinforced concrete structures. Civil engineering and geomechanics series. Wiley, s.l.

25. Zhu H, Hu Y, Ma R et al (2021) Concrete thermal failure criteria, test method, and mechanism: A review. Constr Build Mater 283:122762. https://doi.org/10.1016/j.conbuildmat.2021.122762

26. Kanavaris F, Azenha M, Schlicke D et al (2020) Longitudinal restraining devices for the evaluation of structural behaviour of cement-based materials: the past, present and prospective trends. Strain 56(3):e12343. https://doi.org/10.1111/str.12343

27. Turner K, Schlicke D, Tue NV (2016) Zwangbeanspruchung von Stahlbetonbauteilen. Beton- und Stahlbetonbau 111(5):301–309. https://doi.org/10.1002/best.201600003

28. Shen D, Shi H, Tang X et al (2016) Effect of internal curing with super absorbent polymers on residual stress development and stress relaxation in restrained concrete ring specimens. Constr Build Mater 120:309–320. https://doi.org/10.1016/j.conbuildmat.2016.05.048

29. Nguyen DH, Nguyen VT, Lura P et al (2019) Temperature-stress testing machine—a state-of-the-art design and its unique applications in concrete research. Cem Concr Compos 102:28–38. https://doi.org/10.1016/j.cemconcomp.2019.04.019

30. Cusson D, Hoogeveen T (2007) An experimental approach for the analysis of early-age behaviour of high-performance concrete structures under restrained shrinkage. Cem Concr Res 37(2):200–209. https://doi.org/10.1016/j.cemconres.2006.11.005

31. Springenschmid R, Breitenbücher R, Mangold M (1994) Development of the cracking frame and the temperature stress testing machine. In: Springenschmid R (ed) Thermal cracking in concrete at early ages. CRC Press, pp 137–144

32. Lura P, van Breugel K, Maruyama I (2001) Effect of curing temperature and type of cement on early-age shrinkage of high-

performance concrete. Cem Concr Res 31(12):1867–1872. https://doi.org/10.1016/s0008-8846(01)00601-9

33. Faria R, Leitão L, Teixeira L et al (2017) A structural experimental technique to characterize the viscoelastic behavior of concrete under restrained deformations. Strain 53(1):e12216. https://doi.org/10.1111/str.12216

34. Laube M (1990) Werkstoffmodell zur Berechnung von Temperaturspannungen in massigen Betonbauteilen im jungen Betonalter. Doctoral Thesis, Technische Universität Braunschweig

35. Jonasson J-E, Groth P, Hedlund H (1994) Modelling of temperature and moisture field in concrete to study early age movements as a basis for stress analysis. In: Springenschmid R (ed) Thermal cracking in concrete at early ages. CRC Press, pp 45–52

36. Trost H (1967) Auswirkungen des Superpositionsprinzipes auf Kriech- und Relaxationsprobleme bei Beton und Spannbeton. Beton- und Stahlbetonbau 7(10):230–238

37. Bažant ZP, Baweja S (2000) Creep and shrinkage prediction model for analysis and design of concrete structures: model B3. ACI Spec Publ 194:1–84

38. Bažant ZP (1975) Theory of creep and shrinkage in concrete structures: a precis of recent developments. Mech Today 2(1):1–93

39. Rossi P, Tailhan J-L, Le Maou F (2013) Comparison of concrete creep in tension and in compression: influence of concrete age at loading and drying conditions. Cem Concr Res 51:78–84. https://doi.org/10.1016/j.cemconres.2013.04.001

40. Ranaivomanana N, Multon S, Turatsinze A (2013) Basic creep of concrete under compression, tension and bending. Constr Build Mater 38:173–180. https://doi.org/10.1016/j.conbuildmat.2012.08.024

41. Kovler K (1995) Interdependence of creep and shrinkage for concrete under tension. J Mater Civ Eng 7(2):96–101. https://doi.org/10.1061/(ASCE)0899-1561(1995)7:2(96)

42. Dabarera A, Li L, Dao V (2021) Experimental evaluation and modelling of early-age basic tensile creep in high-performance concrete. Mater Struct 54(3):130. https://doi.org/10.1617/s11527-021-01722-w

43. Bažant ZP, Planas J (1998) Fracture and size effect in concrete and other quasibrittle materials. New directions in civil engineering. CRC Press, Boca Raton, London

44. Eurocode 2 (2011) Design of concrete structures—general rules and rules for buildings 91.010.30; 91.080.40(EN 1992-1-1:2004)

45. Eurocode 2 NA (D) (2013) National annex for Germany—nationally determined parameters—Eurocode 2: design of concrete structures—part 1--1: general rules and rules for buildings 91.010.30; 91.080.40(DIN EN 1992-1-1/NA)

46. Model Code 10 (2013) Fib model code for concrete structures 2010, 1st ed. Ernst Sohn, Berlin

47. Euro-International Committee for Concrete; Fédération internationale de la précontrainte (1993) CEB-FIP model code 1990. Design code. Bulletin d'information/Comité Euro-International du Béton, 213/214. Telford, London

48. Schlicke D, Tue NV (2015) Minimum reinforcement for crack width control in restrained concrete members considering the deformation compatibilty. Stuct Concr 16(2):221–232. https://doi.org/10.1002/suco.201400058

49. Tue NV, Schlicke D (2020) Zwangbeanspruchung und Rissbreitenbeschränkung in Stahlbetonbauteilen auf Grundlage der Verformungskompatibilität. In: Bergmeister K, Fingerloos F, Wörner JD (eds) 2020 Beton Kalender. Wasserbau, Konstruktion und Bemessung, 109. Jahrgang. Ernst & Sohn, a Wiley brand, Berlin, Germany, pp 831–887

50. Cervenka J, Jendele L, Smilauer V (2013) Modelling of crack development in young concrete. In: van Mier J, Ruiz G, Andrade C et al. (eds) 8th International conference on fracture mechanics of concrete structures (FraMCoS-8), Toledo (Spain)

51. Liang M, Chang Z, He S et al (2022) Predicting early-age stress evolution in restrained concrete by thermo-chemo-mechanical model and active ensemble learning. Comput Aided Civ Eng. https://doi.org/10.1111/mice.12915

52. Azenha M, Kanavaris F, Schlicke D et al (2021) Recommendations of RILEM TC 287-CCS: thermo-chemo-mechanical modelling of massive concrete structures towards cracking risk assessment. Mater Struct 54(4):135. https://doi.org/10.1617/s11527-021-01732-8

53. Xu G, Tian Q, Miao J et al (2017) Early-age hydration and mechanical properties of high volume slag and fly ash concrete at different curing temperatures. Constr Build Mater 149:367–377. https://doi.org/10.1016/j.conbuildmat.2017.05.080

54. Gu C, Yao J, Huang S et al (2022) Study on early-age tensile properties of high volume fly ash concrete. Mater Struct 55(5):135. https://doi.org/10.1617/s11527-022-01977-x

55. Caré S (2008) Effect of temperature on porosity and on chloride diffusion in cement pastes. Constr Build Mater 22(7):1560–1573. https://doi.org/10.1016/j.conbuildmat.2007.03.018

56. Kodur V (2014) Properties of concrete at elevated temperatures. ISRN Civ Eng 2014:1–15. https://doi.org/10.1155/2014/468510

57. Shen J, Xu Q, Li Q (2020) Effect of temperature on pore structure and strength of concrete. ACI Mater J. https://doi.org/10.14359/51718060

58. Chan YN, Peng GF, Anson M (1999) Residual strength and pore structure of high-strength concrete and normal strength concrete after exposure to high temperatures. Cem Concr Compos 21(1):23–27. https://doi.org/10.1016/S0958-9465(98)00034-1

59. Bödefeld J, Ehmann R, Schlicke D et al (2012) Mindestbewehrung zur Begrenzung der Rissbreiten in Stahlbetonbauteilen infolge des Hydratationsprozesses. Teil 2: Neues Konzept auf Grundlage der Verformungskompatibilität. Beton-Stahlbetonbau 107(2):79–85. https://doi.org/10.1002/best.201100065

60. Torrenti JM (2018) Basic creep of concrete-coupling between high stresses and elevated temperatures. Eur J Environ Civ Eng 22(12):1419–1428. https://doi.org/10.1080/19648189.2017.1280417

61. Meier A (2015) Der späte Zwang als unterschätzter - aber maßgebender - Lastfall für die Bemessung. Teil 2: Hinweise für Tragwerksplaner. Beton- und Stahlbetonbau 110(3):179–190. https://doi.org/10.1002/best.201400097

62. Fingerloos F, Hegger J (2016) Erläuterungen zur Änderung des deutschen Nationalen Anhangs zu Eurocode 2 (DIN EN 1992–1-1/NA/A1 2015–12). Beton- und Stahlbetonbau 111(1):2–8. https://doi.org/10.1002/best.201500064